J Appl Electrochem (2009) 39:455–461
DOI 10.1007/s10800-008-9693-1

ORIGINAL PAPER

Electrochemical study of the codeposition of Mg–Li–Al alloys from LiCl–KCl–$MgCl_2$–$AlCl_3$ melts

Yong De Yan · Mi Lin Zhang · Yun Xue · Wei Han · Dian Xue Cao · Li Yi He

Received: 1 April 2008 / Accepted: 13 October 2008 / Published online: 25 October 2008

Abstract This work presents a novel electrochemical study on the codeposition of Mg, Li and Al on a molybdenum electrode in LiCl–KCl–$MgCl_2$–$AlCl_3$ melts at 943 K to form Mg–Li–Al alloys. Cyclic voltammograms (CVs) showed that the underpotential deposition (UPD) of magnesium on pre-deposited aluminum leads to the formation of a liquid Mg–Al solution, and the succeeding underpotential deposition of lithium on pre-deposited Mg–Al leads to the formation of a liquid Mg–Li–Al solution. Chronopotentiometric measurements indicated that the codeposition of Mg, Li and Al occurs at current densities lower than -0.47 A cm^{-2} in LiCl–KCl–$MgCl_2$ (0.525 mol kg^{-1}) melts containing 0.075 mol kg^{-1} $AlCl_3$. Chronoamperograms demonstrated that the onset potential for the codeposition of Mg, Li and Al is -2.100 V, and the codeposition of Mg, Li and Al is formed when the applied potentials are more negative than -2.100 V. The diffusion coefficient of aluminum ions in the melts was determined by different electrochemical techniques. X-ray diffraction and inductively coupled plasma analysis indicated that α, $\alpha + \beta$ and β Mg–Li–Al alloys with different lithium and aluminum contents were obtained via potentiostatic and galvanostatic electrolysis.

Y. D. Yan · M. L. Zhang (✉) · Y. Xue · W. Han · D. X. Cao · L. Y. He
Key Laboratory of Superlight Materials and Surface Technology, Ministry of Education, College of Materials Science and Chemical Engineering, Harbin Engineering University, Harbin 150001, China
e-mail: zhangmilin2007@sina.com

Y. D. Yan
e-mail: y5d2004@sina.com

Keywords Mg–Li–Al alloys · KCl–LiCl–$MgCl_2$ · Molten salt · Electrochemical codeposition · Cyclic voltammetry

1 Introduction

Mg–Li based alloys are the lightest among the magnesium alloys, and serve as crucial structural materials for the aerospace industry [1]. These alloys possess excellent cold formability but relatively low strength, especially for those with high lithium contents [2]. Poor corrosion resistance and thermal stability of Mg–Li binary alloys limit their wide application. It has been reported that the addition of some alloying elements, such as Al and/or Zn, enhances their mechanical properties. For instance, the addition of aluminum to Mg–Li based alloys improves their strength due to the formation of intermetallic particles [3].

Mg–Li–Al alloys have become very attractive in recent years because of their low densities and superior mechanical properties [4–8]. Almost all of the Mg–Li–Al alloys are conventionally prepared by directly mixing and fusing the metallic elements. This conventional method has some drawbacks, such as a complicated process of production, problems of oxidation and a high energy cost. Therefore, electrochemical methods for the preparation of magnesium base alloys are drawing increased attention. In our previous work, we successfully prepared Mg–Li alloys on a magnesium cathode from LiCl–KCl melts, and investigated the electrochemical formation process and phase control of Mg–Li alloys at 693–783 K [9, 10]. Lin et al. [11] studied a method of preparing a Mg–Li–Al–Zn alloy on a Mg–Al–Zn cathode by electrodeposition and diffusion of the lithium atoms. However, in these methods, remaining shortcomings include a long process time and high energy

consumption. These drawbacks originate from producing the corresponding metallic cathode materials, and still cannot be eliminated.

Recently, our group proposed a new approach for the direct preparation of Mg–Li–Al alloys via electrochemical codeposition of Mg, Li and Al from LiCl–KCl–$MgCl_2$–$AlCl_3$ melts. The process is simpler than the former methods. Deposition and electrochemical studies of pure metallic magnesium and aluminium have been an area of research. For example, Martínez and co-workers [12–15] have investigated the electrodeposition of magnesium ions in $CaCl_2$–NaCl, $CaCl_2$–NaCl–KCl, eutectic LiCl–KCl and $MgCl_2$–MgF_2 melts. Pal and co-workers [16] reported the electrolytic production of magnesium from magnesium oxide dissolved in fluoride-based fluxes via a solid oxide membrane process. Other researchers [17–19] have investigated the electrochemical parameters of aluminium deposition from alkali chloride melts. However, the codeposition of Mg–Li–Al alloys has not been investigated even though the electrochemical codeposition method has been widely used to prepare other alloys. For example, Ito et al. [20, 21] investigated the electrochemical codeposition of Sm–Co alloys from LiCl–KCl–$SmCl_3$–$CoCl_2$ melts, and electrochemical formation of Yb–Ni and Sm–Ni alloy films by a Li codeposition method on Ni electrode from corresponding chloride melts. Freyland and co-workers [22, 23] reported the preparation of Ni_xAl_{1-x} and Co_xAl_{1-x} alloys via codeposition on Au from room temperature molten salts. Tsuda et al. [24–26] prepared a series of Al-based alloys by codeposition from the molten salts of aluminum chloride-1-ethyl-3-methylimidazolium chloride. Yan et al. [27] investigated the preparation of Mg–Li alloys by codeposition of Mg and Li on an inert electrode from LiCl–KCl–$MgCl_2$ melts.

In this study we investigated the codeposition of Mg–Li–Al alloys from LiCl–KCl–$MgCl_2$–$AlCl_3$ melts by employing a series of electrochemical techniques. The Mg–Li–Al alloys with different phases were prepared by potentiostatic and galvanostatic electrolysis.

2 Experimental

2.1 Preparation and purification of the melts

The LiCl–KCl mixture (63.8:36.2 mol %, analytical grade) was melted in an alumina crucible placed in a quartz cell in an electric furnace. The temperature of the melts was measured with a nickel–chromium thermocouple sheathed by an alumina tube. The mixture was dried under vacuum for more than 72 h at 473 K to remove excess water. Metal ion impurities in the melts were removed by pre-electrolysis at −2.0 V (vs. Ag/AgCl) for 4 h. Magnesium and aluminum ions were introduced into the bath in the form of dehydrated $MgCl_2$ and $AlCl_3$ powder. All experiments were performed under an argon atmosphere.

2.2 Electrochemical apparatus and electrodes

All electrochemical measurements were performed using an Im6eX electrochemical workstation (Zahner Co., Ltd.) with a THALES 3.08 software package. A silver wire ($d = 1$ mm) dipped into a Pyrex tube containing a solution of AgCl (0.070 mol kg^{-1}) in LiCl–KCl melts was used as a reference electrode (Ag/AgCl couple) for all potentials. The working electrodes were molybdenum wires ($d = 1$ mm, 99.99% purity). A spectrally pure graphite rod ($d = 6$ mm) served as the counter electrode. The molybdenum working electrode was polished thoroughly using SiC paper, and then cleaned ultrasonically with ethanol. After each experiment, the active electrode surface was determined by measuring the immersion depth of the electrode in the molten salts.

2.3 Auxiliary techniques

The samples of Mg–Li–Al alloys were prepared by potentiostatic and galvanostatic electrolysis under different conditions. After electrolysis, all samples were washed in hexane (99.8% purity) in an ultrasonic bath to remove salts and stored in a glove box for analysis. These deposits were analyzed by XRD (X' Pert Pro; Philips Co., Ltd.) using Cu–Kα radiation at 40 kV and 40 mA. In order to determine the Li and Al contents of the samples, each sample was dissolved in aqua regia (HNO_3:HCl:H_2O = 1:3:8, v/v). The solution was diluted and analyzed using an inductively coupled plasma atomic emission spectrometer (ICP-AES, Thermo Elemental, IRIS Intrepid II XSP).

3 Results and discussion

3.1 Cyclic voltammetry

Figure 1 shows typical CVs obtained at a molybdenum electrode before and after the addition of 0.525 mol kg^{-1} $MgCl_2$ and 0.075 mol kg^{-1} $AlCl_3$ in LiCl–KCl melts (63.8:36.2 mol %) at 943 K. The dotted curve represents the voltammogram before the addition of $MgCl_2$ and $AlCl_3$. Only one couple of cathodic/anodic signals is observed which corresponds to the deposition and dissolution of liquid Li. The solid curves show the voltammograms at different cathodic limits after the addition of $MgCl_2$ and $AlCl_3$. Since the deposition potential of Al ions is more positive than that of Mg ions in a chloride system [28], peak A and peak B in the forward

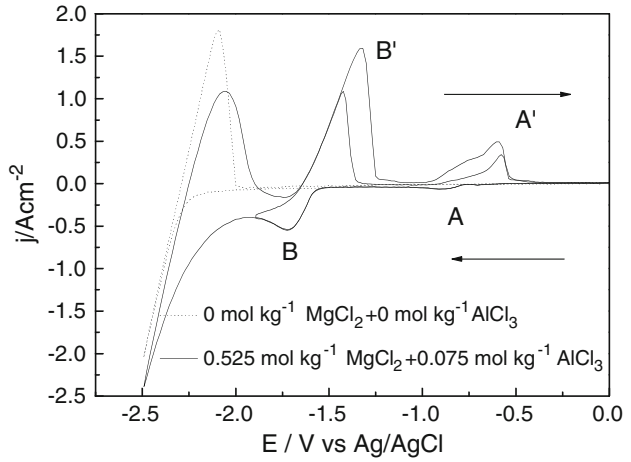

Fig. 1 Typical CVs of the LiCl–KCl melts before and after the addition of 0.525 mol kg^{-1} $MgCl_2$ and 0.075 mol kg^{-1} $AlCl_3$ on a molybdenum electrode at 943 K. Scan rate: 0.1 V s^{-1}

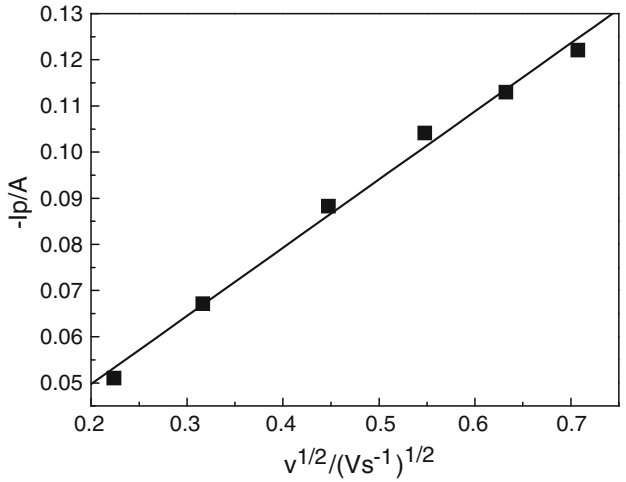

Fig. 3 Variation of cathodic peak current as a function of the potential scan rate on a molybdenum electrode (0.4789 cm^2) in the LiCl–KCl–$MgCl_2$ (0.525 mol kg^{-1}) melts with 0.075 mol kg^{-1} $AlCl_3$ at 943 K

scan are ascribed to a three-dimensional (3D) phase formation [22] of Al and Mg electrodeposition (i.e. overpotential deposition), respectively. In the reverse scan, excluding the anodic peak corresponding to oxidation of liquid lithium, the profile of peaks B′ and A′ clearly indicates the dissolution reactions of deposited Mg and Al. These peaks also show oxidation reactions of the alloys. For example, an anodic current wave prior to peak A′ corresponds to the oxidation reactions of Mg–Al alloys.

Figure 2 shows CVs obtained for 0.075 mol kg^{-1} $AlCl_3$ (1.14×10^{-4} mol cm^{-3}) in LiCl–KCl–$MgCl_2$ (0.525 mol kg^{-1}) melts on a molybdenum electrode at different scan rates at 943 K. A pair of cathodic/anodic peaks is observed which corresponds to the deposition and dissolution of Al. The peak currents (I_p) increase with the increase of scan rate (v). Figure 3 gives the plot of I_p against $v^{1/2}$. It can be seen that I_p and $v^{1/2}$ shows a linear relationship, which

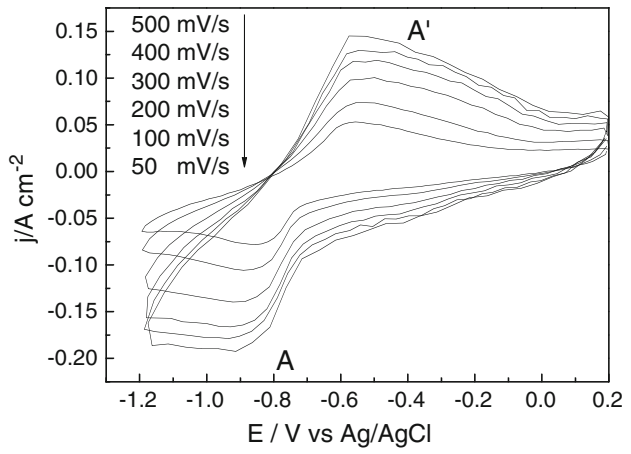

Fig. 2 CVs of the LiCl–KCl–$MgCl_2$ (0.525 mol kg^{-1}) melts with 0.075 mol kg^{-1} $AlCl_3$ on a molybdenum electrode (0.4789 cm^2) at different scan rates at 943 K

indicates that the electrode process of Al(III) ions is controlled by rate of the mass transfer. The diffusion coefficient of the Al(III) ions was calculated using the Berzins–Delahay equation for soluble–insoluble systems [29]:

$$I_p = 0.61(nF)^{3/2} S C_0 D^{1/2} v^{1/2} (RT)^{-1/2} \quad (1)$$

where S is the electrode surface area in cm^2, C is the solute concentration in mol cm^{-3}, D is the diffusion coefficient in cm^2 s^{-1}, F is Faraday's constant (96,485 C mol^{-1}), R is the universal gas constant, n is the number of exchanged electrons, v is the potential sweep rate in V s^{-1}, and T is the absolute temperature in K. The calculation of the diffusion coefficient using Eq. 1 yields $D_{Al(III)} = 0.65(\pm 0.07) \times 10^{-5}$ cm^2 s^{-1}. For a reversible electrode reaction involving the deposition of an insoluble substance, $|E_p - E_{p/2}|$ (where $E_{p/2}$ is the half-peak potential) should have a value of $0.7725RT/nF$ or 0.021 V for a three-electron reaction at 943 K [18]. However in this case, $|E_p - E_{p/2}|$ is found to exceed 0.021 V. Besides, the cathodic peak potential shifts slightly towards negative values as the sweep rate is increased. These observations suggest that the Al(III) deposition/dissolution reaction is not completely reversible.

Figure 4 shows CVs obtained at a molybdenum electrode in LiCl–KCl–$MgCl_2$ (0.525 mol kg^{-1}) melts containing $AlCl_3$ with different concentrations at 943 K. When compared to curve 1, an obvious cathodic current can be seen between peak A and B in curves 2 and 3. With reference to the phase diagram of the Mg–Al system [30] the cathodic current is likely due to the formation of a Mg–Al alloy. Peak B is associated with the reduction of Mg(II) ions on the Mg–Al pre-deposited on the molybdenum electrode. The

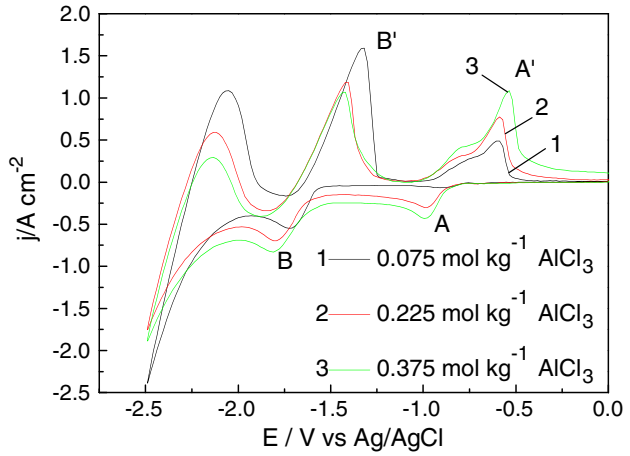

Fig. 4 CVs of the LiCl–KCl–$MgCl_2$ (0.525 mol kg^{-1}) melts containing different $AlCl_3$ concentrations at a molybdenum electrode at 943 K. Scan rate: 0.1 V s^{-1}

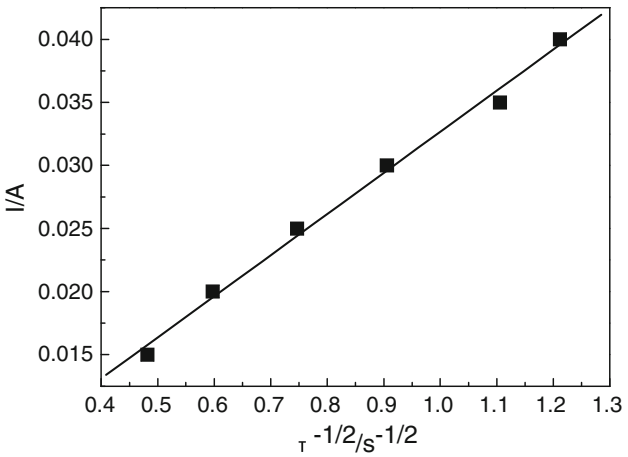

Fig. 6 The plot of I vs. $\tau^{1/2}$ for the reduction of Al(III) in the LiCl–KCl–$MgCl_2$ (0.525 mol kg^{-1}) melts. Electrode area: 0.3847 cm^2; temperature: 943 K; concentration of $AlCl_3$: 0.075 mol kg^{-1} (1.14×10^{-4} mol cm^{-3})

underpotential deposition of lithium on pre-deposited Mg–Al leads to the formation of a liquid Mg–Li–Al solution at 943 K. In addition, the difference in peak potentials between the reduction and oxidation of Al and Mg increases with the increase of $AlCl_3$ concentration, indicating that the electrode processes of Al and Mg are more irreversible at high $AlCl_3$ concentration.

3.2 Chronopotentiometry

Figure 5 shows chronopotentiograms measured on a molybdenum electrode ($S = 0.3847$ cm^2) in LiCl–KCl–$MgCl_2$ (0.525 mol kg^{-1}) melts containing 0.075 mol kg^{-1} $AlCl_3$ at different current intensities. At a cathodic current lower than −20 mA (current density −0.052 A cm^{-2}), the curves exhibit two potential plateaus (plateaus 1 and 2), which are associated with the reduction of aluminum

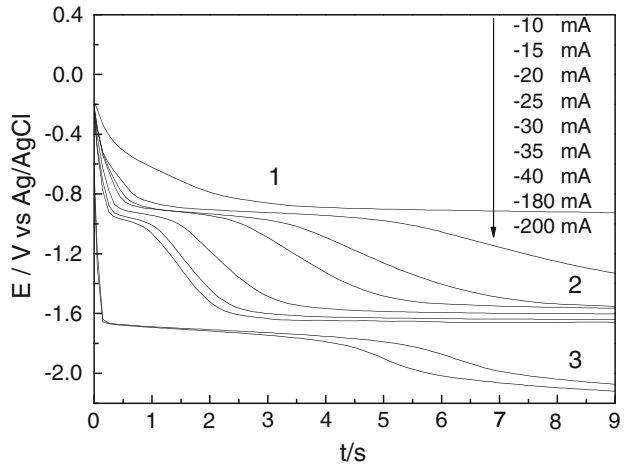

Fig. 5 Chronopotentiograms obtained at different current intensities on a molybdenum electrode (0.3847 cm^2) in the LiCl–KCl–$MgCl_2$ (0.525 mol kg^{-1}) melts containing 0.075 mol kg^{-1} $AlCl_3$ at 943 K

(plateau 1) and magnesium (plateau 2) ions to metals. When the current reaches −180 mA (−0.47 A cm^{-2}), a third plateau appears caused by the reduction of lithium ions. At this current intensity, codeposition of Mg, Li and Al occurs. It is obvious that the potential ranges for the deposition of Mg, Li and Al are the same as those observed in the cyclic voltammograms.

The transition time, τ, was determined by the duration of plateau 1 in the chronopotentiograms between −15 and −40 mA using the methodology described in Ref. [31]. Several current intensities were applied, and the plot of I vs. $\tau^{-1/2}$ exhibits a linear relationship as shown in Fig. 6. In addition, the chronopotentiograms do not shift towards negative potentials with the increasing current intensity. Based on these results, it can be concluded that the electrochemical reduction of Al(III) ions is diffusion controlled [32]. The diffusion coefficient of Al(III) in the LiCl–KCl melts was calculated using Sand's equation [33]:

$$I\tau^{1/2} = \frac{nFSC_0D^{1/2}\pi^{1/2}}{2} \quad (2)$$

where τ is the transition time measured in the chronopotentiograms, and S, C_0 and D have the same meanings and units as described in Eq. 1. The value of the diffusion coefficient, $D_{Al(III)}$, calculated using Eq. 2 is $0.84(\pm 0.06) \times 10^{-5}$ cm^2 s^{-1}, which is in good agreement with the value obtained by cyclic voltammetry in Sect. 3.1.

3.3 Chronoamperometry

Chronoamperometry was employed to further investigate the electrochemical formation of Mg–Li–Al alloys via codeposition of Mg, Li and Al. The chronoamperometric curves show typical features of a reduction process

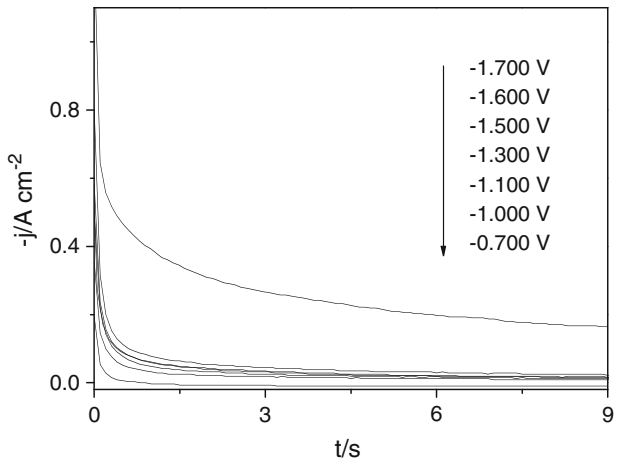

Fig. 7 Chronoamperograms for the LiCl–KCl–$MgCl_2$ (0.525 mol kg^{-1}) melts containing 0.075 mol kg^{-1} $AlCl_3$ on a molybdenum electrode (0.3847 cm^2) at various applied potentials at 943 K

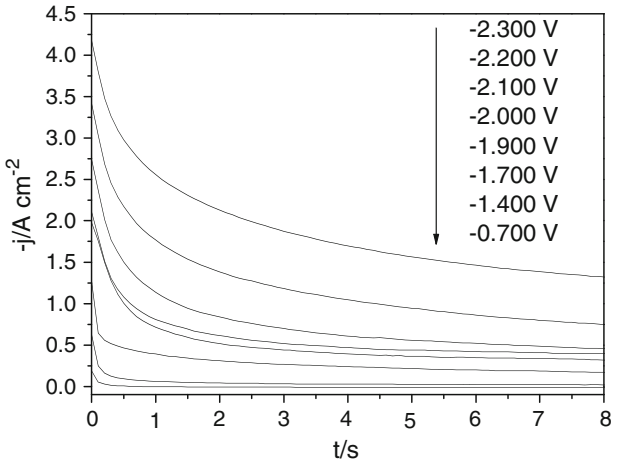

Fig. 8 Chronoamperograms for the LiCl–KCl–$MgCl_2$ (0.525 mol kg^{-1}) melts containing 0.075 mol kg^{-1} $AlCl_3$ on a molybdenum electrode (0.3847 cm^2) at more negative applied potentials at 943 K

controlled by planar diffusion (see Fig. 7). It is obvious that the total current density sharply increases at an applied potential of −1.700 V, indicating that the reduction of Al(III) is accompanied by that of Mg(II). For a planar electrode, the Cottrell equation [33] is given as follows:

$$i = -\frac{nFAD^{1/2}C_0}{\pi^{1/2}t^{1/2}} \tag{3}$$

The current falls as $t^{-1/2}$ in the potential range of −1.000 to −1.600 V for the reduction of Al(III), and a plot of I vs. $t^{-1/2}$ should therefore be linear and pass through the origin (this is frequently used for a diagnosis of diffusion control) [34]. However, this relationship is only satisfied in the region of −1.300 to −1.500 V. Superposition of the curves in the interval of −1.300 to −1.500 V also indicates the validity of the Cottrell equation. Accordingly, the calculation of the diffusion coefficient using Eq. 3 yields $D_{Al(III)} = 2.87(\pm 0.09) \times 10^{-5}$ cm^2 s^{-1}. The values of diffusion coefficients of Al(III) obtained by three electrochemical techniques are summarized in Table 1. The discrepancy in the diffusion coefficients between this work and data reported in the literature [17, 18] in MCl–$AlCl_3$ melts (M = Na, K, Cs) might be due to different experimental temperatures and uncertainties caused by different melt systems. Figure 8 shows chronoamperometry with increased applied potentials on a molybdenum electrode. The total current density increases rapidly when the step potential changes from −2.000 to −2.100 V, which shows that Li (I) also starts to be reduced. Accordingly, codeposition of Mg, Li and Al can occur when the applied potential is more negative than −2.100 V. In addition, the potential ranges of deposition of Mg, Li and Al are the same as those observed in the cyclic voltammograms and chronopotentiograms.

Table 1 Diffusion coefficient (D 10^5 cm^2 s^{-1}) of Al(III) species obtained by different electrochemical techniques in the LiCl–KCl–$MgCl_2$ (0.525 mol kg^{-1}) mixture at 943 K

Technique	D 10^5 cm^2 s^{-1}
Cyclic voltammetry	0.65 ± 0.07
Chronopotentiometry	0.84 ± 0.06
Chronoamperometry	2.87 ± 0.09

3.4 Potentiostatic electrolysis and characterization of the deposits

Based on the results obtained by CVs, chronopotentiometrys and chronoamperometrys, potentiostatic and galvanostatic

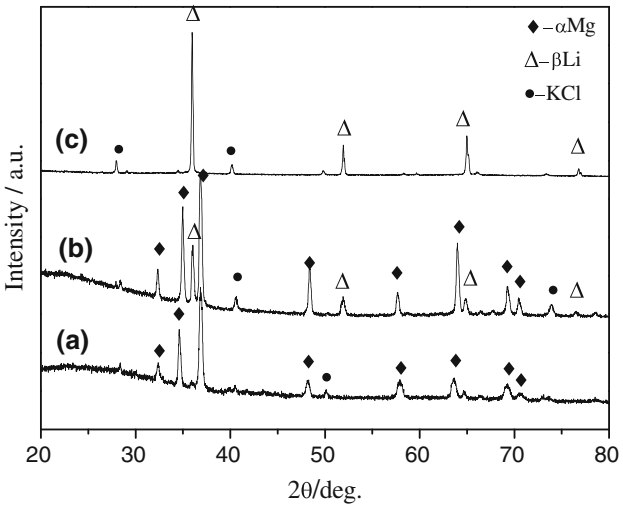

Fig. 9 XRD patterns of deposits obtained by potentiostatic electrolysis on Mo electrodes in the LiCl–KCl–$MgCl_2$ (0.525 mol kg^{-1}) melts containing 0.225 mol kg^{-1} $AlCl_3$ at (a) −2.40 V; (b) −2.45 V; (c) −2. 50 V for 2 h

electrolysis were carried out in LiCl–KCl melts containing $MgCl_2$ and $AlCl_3$ with different concentrations on molybdenum electrodes at 943 K. Figure 9 shows the XRD patterns of typical α, $\alpha + \beta$ and β Mg–Li–Al alloy phases obtained by potentiostatic electrolysis from the LiCl–KCl–$MgCl_2$ (0.525 mol kg^{-1}) melts containing 0.225 mol kg^{-1} $AlCl_3$ at −2.4, −2.45 and −2.5 V for 2 h, respectively. Al has no apparent effect on the phase structure of Mg–Li alloys because of relatively low Al contents in Mg–Li–Al alloys. It is obvious that the lithium contents of the Mg–Li–Al alloys increase (from α to β phase) with negative shifts in the applied potential. The ICP analyses of all samples obtained by potentiostatic and galvanostatic electrolysis are listed in Tables 2 and 3, respectively. Under potentiostatic electrolysis, the more negative the applied potential in the LiCl–KCl–$MgCl_2$ (0.525 mol kg^{-1}) melts with equivalent $AlCl_3$ concentration, the higher the lithium content of Mg–Li–Al alloy. In addition, the aluminum contents of Mg–Li–Al alloys increase with increasing $AlCl_3$ concentrations in LiCl–KCl–$MgCl_2$ (0.525 mol kg^{-1}) melts. Under galvanostatic electrolysis, the lower $MgCl_2$ concentration in the LiCl–KCl melts with equivalent $AlCl_3$ concentration at a constant current intensity, the higher the lithium content of the Mg–Li–Al alloys. The aluminum contents of Mg–Li–Al alloys increase with the increase of $AlCl_3$ concentrations in LiCl–KCl–$MgCl_2$ melts. These results indicate that the lithium and aluminum contents of Mg–Li–Al alloys are adjustable simply by changing the concentrations of $MgCl_2$ and $AlCl_3$ and the electrolytic parameters.

Table 2 The ICP analyses of all samples obtained by potentiostatic electrolysis on Mo electrodes from the LiCl–KCl–$MgCl_2$ (0.525 mol kg^{-1}) melts for 2 h

Samples	$AlCl_3$ concentration (mol kg^{-1})	Electrolytic potential (V)	Al content (at.%)	Li content (at.%)
1	0.075	−2.50	0.31	86.38
2	0.225	−2.40	0.99	3.55
3	0.225	−2.45	0.63	29.16
4	0.225	−2.50	0.65	68.98
5	0.375	−2.50	2.23	4.12
6	0.375	−2.60	1.03	79.65

Table 3 The ICP analyses of all samples obtained by galvanostatic electrolysis (2 A) on Mo electrodes ($S = 0.322$ cm^2) from the LiCl–KCl melts containing different $MgCl_2$ and $AlCl_3$ concentrations for 2 h

Samples	$MgCl_2$ concentration (mol kg^{-1})	$AlCl_3$ concentration (mol kg^{-1})	Al content (at.%)	Li content (at.%)
1	0.525	0.075	0.08	90.35
2	0.735	0.075	0.04	77.66
3	0.840	0.075	0.05	67.97
4	0.945	0.075	0.35	17.56
5	0.525	0.225	0.74	81.33
6	0.525	0.375	1.66	62.09
7	0.735	0.375	1.91	14.87
8	0.840	0.375	2.44	5.63
9	0.945	0.375	2.42	2.89

4 Conclusions

The electrochemical codeposition behavior of Mg, Li and Al on a Mo electrode, in LiCl–KCl (63.8:36.2 mol %) melts containing different concentrations of $MgCl_2$ and $AlCl_3$ at 943 K, was investigated. The electrode process of Al(III) ions in LiCl–KCl melts containing 0.525 mol kg^{-1} $MgCl_2$ is controlled by the rate of mass transfer, and some irreversibility is involved in the process. From the current work, Mg–Li–Al alloys can be directly prepared via co-deposition of Mg, Li and Al on inert electrodes from LiCl–KCl–$MgCl_2$–$AlCl_3$ melts. α, $\alpha + \beta$ and β Mg–Li–Al alloys with different lithium and aluminum contents were obtained by potentiostatic and galvanostatic electrolysis on molybdenum electrodes at 943 K. The lithium and aluminum contents of Mg–Li–Al alloys can be controlled by $MgCl_2$ and $AlCl_3$ concentrations and the electrolytic parameters. Mg–Li–Al alloys prepared directly from $MgCl_2$, LiCl and $AlCl_3$ could revolutionize the Mg–Li–Al alloy industry.

Acknowledgments The work was financially supported by the National 863 Project of the Ministry of Science and Technology of China (2006AA03Z510), the Scientific Technology Project of Heilongjiang Province (GC06A212), the National Natural Science Foundation of China (50871033) and the Scientific Technology Bureau of Harbin (2006PFXXG006). The authors are particularly grateful to Professors Tom Mann and Justin Cheney for kindly discussing various parts of the manuscript.

References

1. Haferkamp H, Niemeyers M, Boehm R, Holzkamp U, Jaschik C, Kaese V (2000) Mater Sci Forum 350–351:31
2. Jackson JH, Frost PD, Loonam AC, Eastwood LW, Lorig CH (1949) Met Trans 185:149
3. Liu T, Wu SD, Li SX, Li PJ (2007) Mater Sci Eng A 460–461:499
4. Liu T, Wu SD, Jiang CB, Li SX, Xu YB (2003) Mater Sci Eng A 360:345
5. Kim YW, Kim DH, Lee HI, Hong CP (1998) Scripta Mater 38:923
6. Drozd Z, Trojanová Z, Kúdela S (2004) J Alloys Compd 378:192
7. Drozd Z, Trojanová Z, Kúdela S (2007) Mater Sci Eng A 462:234
8. Murken J, Höhner R, Skrotzki B (2003) Mater Sci Eng A 363:159

9. Zhang ML, Yan YD, Hou ZY, Fan LA, Chen Z, Tang DX (2007) J Alloys Compd 440:362
10. Yan YD, Zhang ML, Han W, Cao DX, Yuan Y, Xue Y, Chen Z (2008) Electrochim Acta 53:3323
11. Lin MC, Tsai CY, Uan JY (2007) Scripta Mater 56:597
12. Castrillejo Y, Martínez AM, Pardo R, Haarberg GM (1997) Electrochim Acta 42:1869
13. Martínez AM, Børresen B, Haarberg GM, Castrillejo Y, Tunold R (2004) J Electrochem Soc 151:C508
14. Martínez AM, Børresen B, Haarberg GM, Castrillejo Y, Tunold R (2004) J Appl Electrochem 34:1271
15. Børresen B, Haarberg GM, Tunold R (1997) Electrochim Acta 42:1613
16. Krishnan A, Lu XG, Pal UB (1985) Metall Mater Trans B 36:463
17. Gabčo M, Fellner P, Lubyová Ž (1984) Electrochim Acta 29:397
18. Ødegard R, Bjørgum A, Sterten Å, Thonstad J, Tunold R (1982) Electrochim Acta 27:1595
19. Schulze K, Hoff H (1972) Electrochim Acta 17:119
20. Iida T, Nohira T, Ito Y (2003) Electrochim Acta 48:2517
21. Iida T, Nohira T, Ito Y (2003) Electrochim Acta 48:1531
22. Freyland W, Zell CA, Zein El Abedin S, Endres F (2003) Electrochim Acta 48:3053
23. Zell CA, Freyland W (2001) Chem Phys Lett 337:293
24. Tsuda T, Hussey CL, Stafford GR, Bonevich JE (2003) J Electrochem Soc 150:C234
25. Tsuda T, Hussey CL, Stafford GR (2004) J Electrochem Soc 151:C379
26. Tsuda T, Hussey CL, Stafford GR, Kongstein O (2004) J Electrochem Soc 151:C447
27. Yan YD, Zhang ML, Han W, Xue Y, Cao DX, Yuan Y (2008) Chem Lett 37:212
28. Yang QQ, Fang BL, Tong YX (2005) Applied electrochemistry, 2nd edn. Zhongshan University Press, Guangzhou
29. Berzins T, Delahay P (1953) J Am Chem Soc 75:555
30. Massalski TB, Murray JL, Benett LH, Baker H (1990) Binary alloy phase diagrams. American Society for Metals, Metals Park
31. Laity RW, McIntyre JDE (1965) J Am Chem Soc 87:3806
32. Galus Z (1976) Fundamentals of electrochemical analysis. Ellis Horwood, London
33. Bard AJ, Faulkner LR (1980) Electrochemical methods: fundamentals and applications. Wiley, New York
34. Group Southampton Electrochemistry (1985) Instrumental methods in electrochemistry. Ellis Horwood, Chichester